

CHMP1A encodes an essential regulator of BMI1-INK4A in cerebellar development

Ganeshwaran H Mochida^{1-5,18}, Vijay S Ganesh^{1-3,6,18}, Maria I de Michelena⁷, Hugo Dias⁸, Kutay D Atabay¹⁻³, Katie L Kathrein^{3,9-11}, Hsuan-Ting Huang^{3,9-11}, R Sean Hill¹⁻³, Jillian M Felie¹⁻³, Daniel Rakiec¹⁻³, Danielle Gleason¹⁻³, Anthony D Hill¹², Athar N Malik⁶, Brenda J Barry¹⁻³, Jennifer N Partlow¹⁻³, Wen-Hann Tan^{1,4}, Laurie J Glader^{4,13}, A James Barkovich¹⁴, William B Dobyns¹⁵, Leonard I Zon^{3,4,9-11,16} & Christopher A Walsh^{1-4,17}

Charged multivesicular body protein 1A (CHMP1A; also known as chromatin-modifying protein 1A) is a member of the ESCRT-III (endosomal sorting complex required for transport-III) complex^{1,2} but is also suggested to localize to the nuclear matrix and regulate chromatin structure³. Here, we show that loss-of-function mutations in human *CHMP1A* cause reduced cerebellar size (pontocerebellar hypoplasia) and reduced cerebral cortical size (microcephaly). *CHMP1A*-mutant cells show impaired proliferation, with increased expression of *INK4A*, a negative regulator of stem cell proliferation. Chromatin immunoprecipitation suggests loss of the normal *INK4A* repression by BMI in these cells. Morpholino-based knockdown of zebrafish *chmp1a* resulted in brain defects resembling those seen after *bmi1a* and *bmi1b* knockdown, which were partially rescued by *INK4A* ortholog knockdown, further supporting links between CHMP1A and BMI1-mediated regulation of *INK4A*. Our results suggest that CHMP1A serves as a critical link between cytoplasmic signals and BMI1-mediated chromatin modifications that regulate proliferation of central nervous system progenitor cells.

As part of ongoing studies of human disorders affecting neural progenitor proliferation, we identified three families characterized by underdevelopment of the cerebellum, pons and cerebral cortex (Fig. 1a–d). In a consanguineous pedigree of Peruvian origin, three children in two branches were affected (Fig. 1e, family 1). Two additional pedigrees from Puerto Rico showed similar pontocerebellar hypoplasia and microcephaly (Fig. 1e, families 2 and 3). Brain magnetic resonance imaging (MRI) of affected individuals from all families showed

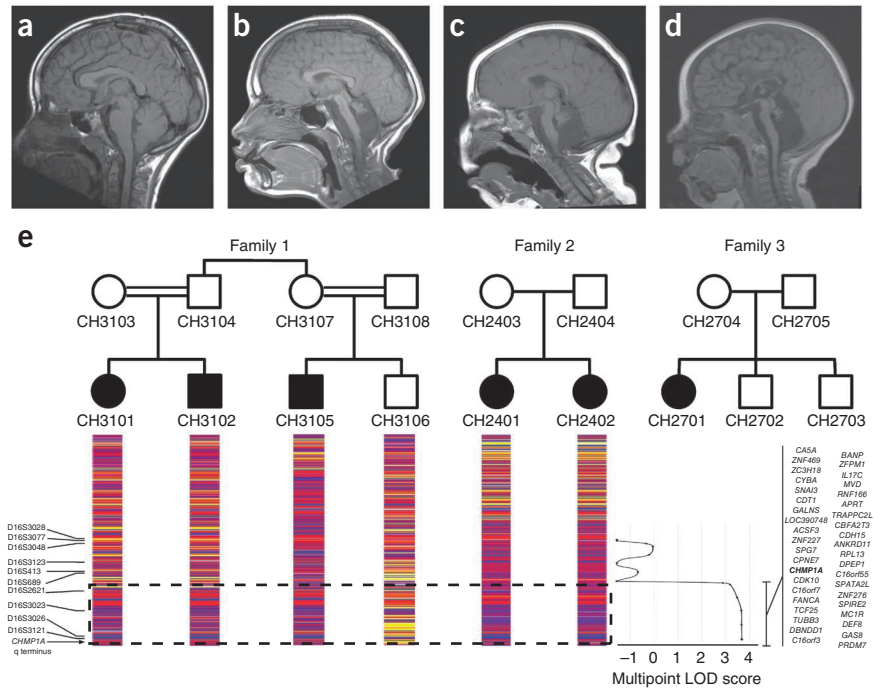
severe reduction of the cerebellar vermis and hemispheres relative to normal individuals. Notably, the cerebellar folds (folia) were relatively preserved, despite the extremely small cerebellar size (Fig. 1a–d and Supplementary Videos 1 and 2). All affected individuals had severe pontocerebellar hypoplasia, although affected individuals in family 1 showed better motor and cognitive function than those in families 2 and 3 (Supplementary Note).

Genome-wide linkage analysis of families 1 and 2 using SNP microarrays implicated only one region on chromosome 16q as linked and homozygous in all six affected individuals (Fig. 1e and Supplementary Fig. 1), with a maximum multipoint logarithm of odds (LOD) score of 3.68 (Fig. 1e). Although families 2 and 3 are not highly informative for linkage analysis, their shared homozygosity provides additional support for the involvement of this locus. Furthermore, families 2 and 3 shared the same haplotype (Supplementary Fig. 1), suggesting a founder effect. Sequencing of 42 genes within the candidate interval at 16q24.3 revealed homozygous variants predicted to be deleterious only in the *CHMP1A* gene. *CHMP1A* (NM_002768) consists of seven exons encoding a 196-amino-acid protein (Supplementary Note). Affected individuals in families 2 and 3 had a homozygous nonsense variant in exon 3 predicted to prematurely terminate translation (c.88C>T, p.Gln30*; Fig. 2a,b). Family 1 showed a homozygous variant in intron 2 of *CHMP1A* (c.28–13G>A; Fig. 2a,b) predicted to create an aberrant splice acceptor site leading to an 11-bp insertion in the spliced mRNA product (Supplementary Fig. 2a). The two mutations were absent from dbSNP, 281 neurologically normal European control DNA samples (562 chromosomes), the 1000 Genomes Project database⁴ and approximately 5,000 control exomes from the National Heart, Lung, and Blood Institute (NHLBI) Exome Sequencing Project.

¹Department of Medicine, Division of Genetics, Boston Children's Hospital, Boston, Massachusetts, USA. ²Manton Center for Orphan Disease Research, Boston Children's Hospital, Boston, Massachusetts, USA. ³Howard Hughes Medical Institute, Boston Children's Hospital, Boston, Massachusetts, USA. ⁴Department of Pediatrics, Harvard Medical School, Boston, Massachusetts, USA. ⁵Pediatric Neurology Unit, Department of Neurology, Massachusetts General Hospital, Boston, Massachusetts, USA. ⁶Harvard–Massachusetts Institute of Technology (MIT) Division of Health Sciences and Technology, Cambridge, Massachusetts, USA. ⁷Department of Morphologic Sciences, Cayetano Heredia University, Lima, Peru. ⁸Institute for Child Development–ARIE, Lima, Peru. ⁹Stem Cell Program, Boston Children's Hospital, Boston, Massachusetts, USA. ¹⁰Division of Hematology/Oncology, Boston Children's Hospital, Boston, Massachusetts, USA. ¹¹Dana-Farber Cancer Institute, Boston, Massachusetts, USA. ¹²Department of Neurology, Boston Children's Hospital, Boston, Massachusetts, USA. ¹³Complex Care Service, Division of General Pediatrics, Boston Children's Hospital, Boston, Massachusetts, USA. ¹⁴Department of Radiology and Biomedical Imaging, University of California, San Francisco, San Francisco, California, USA. ¹⁵Center for Integrative Brain Research, University of Washington, Seattle, Washington, USA. ¹⁶Harvard Stem Cell Institute, Cambridge, Massachusetts, USA. ¹⁷Department of Neurology, Harvard Medical School, Boston, Massachusetts, USA. ¹⁸These authors contributed equally to the work. Correspondence should be addressed to C.A.W. (christopher.walsh@childrens.harvard.edu).

Received 7 May; accepted 5 September; published online 30 September 2012; doi:10.1038/ng.2425

Figure 1 Brain MRI and linkage mapping of pontocerebellar hypoplasia with microcephaly. (a–d) T1-weighted sagittal brain MRIs of a neurologically normal individual (a) and affected individuals CH3102 (b), CH2402 (c) and CH2701 (d). Compared to control, affected individuals show mild reduction in cortical volume, thinning of the corpus callosum and severe hypoplasia of the pons, cerebellar vermis and cerebellar hemispheres. (e) Family 1 is a consanguineous pedigree from Peru in which three children from two branches are affected. Families 2 and 3 are both from Puerto Rico. Affymetrix 250K Sty SNP data for each child in families 1 and 2 are shown below (red or blue, homozygous SNP call; yellow, heterozygous SNP call), showing a region of homozygosity (dashed box) shared by all affected individuals in distal chromosome 16q. The graph aligned with the SNP genotyping data shows multipoint LOD scores calculated from microsatellite maker analysis of family 1 (**Supplementary Fig. 1**). Genes in the region of LOD of >3 are indicated to the right of the graph.



We sequenced *CHMP1A* in 64 individuals with other cerebellar anomalies without finding additional mutations, but none of these affected individuals shared the rare and distinctive pattern of hypoplasia seen in the individuals with *CHMP1A* mutations.

RT-PCR analysis of *CHMP1A* in lymphoblastoid cells from affected individuals from family 1 (CH3101 and CH3105) identified the predicted aberrant transcript with the 11-bp insertion and a second aberrant transcript with a 21-bp insertion but no normal *CHMP1A* transcript (**Supplementary Fig. 2b**). In the parents of affected children from family 1 and in unaffected control samples, only the normal transcript was detected, suggesting that the abnormal splice products

are unstable. Protein blot analysis revealed a single 24-kDa band in a normal control individual, but no corresponding band was detected in affected individuals from families 1 and 2 (CH3101 and CH2401, respectively; **Fig. 2c**). In the parent (CH3103), the amount of CHMP1A was 50% relative to the amount detected in control lysate. Hence, this genetic study establishes *CHMP1A* null mutations as the cause of pontocerebellar hypoplasia and microcephaly in these pedigrees.

CHMP1A has been assigned two distinct putative functions as both a chromatin-modifying protein and a charged multivesicular

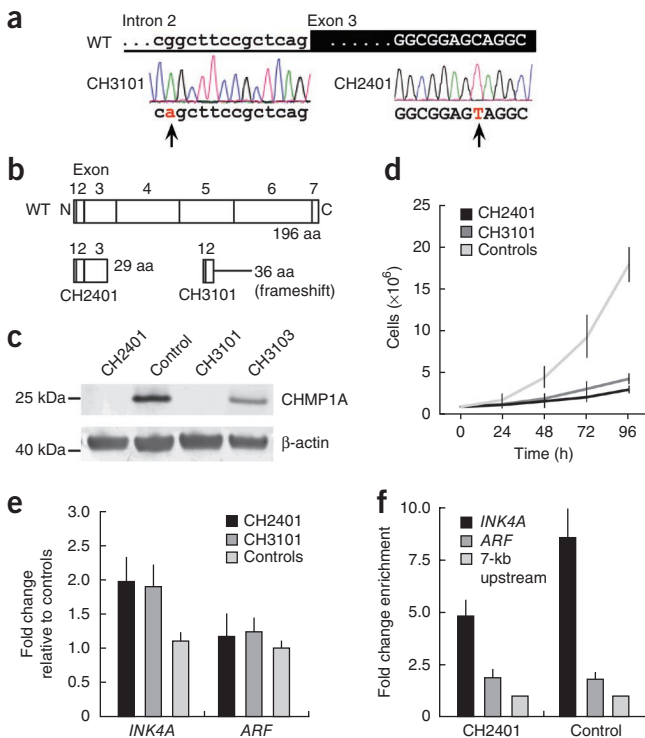


Figure 2 Loss-of-function mutations in *CHMP1A* and dysregulation of *INK4A* in cell lines from affected individuals. (a) Chromatograms showing homozygous mutations (red, indicated by arrows) in intron 2 (CH3101; c.28–13G>A; white background) and in exon 3 (CH2401; c.88C>T; black background) of *CHMP1A*. (b) Schematic of full-length wild-type (WT) *CHMP1A*. The mutation in CH2401 leads to premature termination of translation. The intronic mutation in CH3101 creates a novel splice acceptor site, and usage of this novel acceptor site causes a frameshift after exon 2, resulting in termination of translation after 36 amino acids. (c) Protein blotting of lysates from lymphoblastoid cell lines from CH2401 and CH3101 showing a complete loss of the 24-kDa band detected by antibody to CHMP1A in control lysate. Lysate from a cell line generated from CH3103 (the mother of CH3101) show 50% of the protein amount relative to the control. Protein amounts were normalized to the 40-kDa β -actin loading control bands. (d) Lymphoblastoid cell lines from CH2401 and CH3101 proliferate at a much lower rate than eight control cell lines. (e) qPCR analysis of *CDKN2A*-derived cDNA levels in human lymphoblastoid cell lines from CH2401 and CH3101 (normalized to *GAPDH* levels) shows nearly twofold higher expression of *INK4A* in these cells relative to four unrelated, neurologically normal control cell lines. The other transcribed isoform at the locus, *ARF*, shows no significant difference in expression in cells from affected individuals and control cells. (f) ChIP-qPCR in lymphoblastoid cell lines using an antibody to BMI1 shows an approximately eightfold enrichment of *INK4A* promoter DNA relative to a probe targeted 7-kb upstream of the locus in a control cell line. Enrichment is nearly half of this in cell lines derived from CH2401 with a homozygous mutation in *CHMP1A*. Enrichment at the *ARF* promoter is not significantly different from that observed in the control cell line. Error bars in d–f, s.e.m.

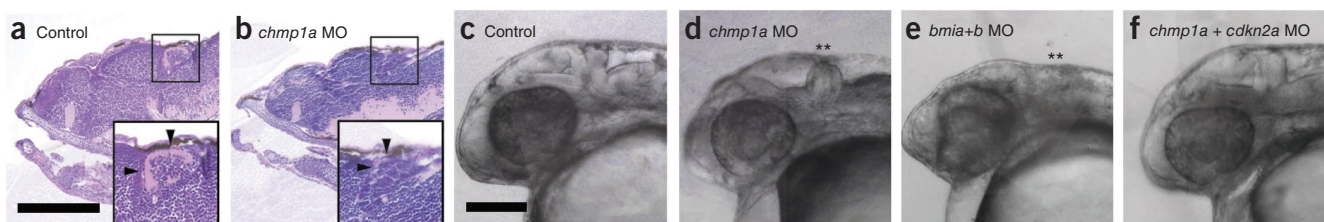
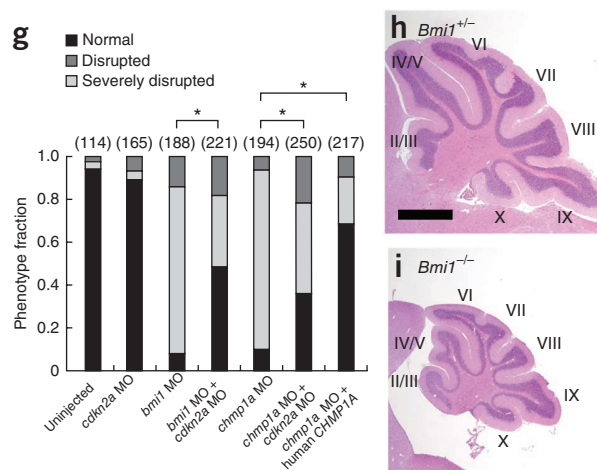


Figure 3 Genetic links between *CHMP1A* and *BMI1* in zebrafish and mice. (a,b) In parasagittal sections at 5 days post-fertilization (d.p.f.), zebrafish injected with *chmp1a* morpholino (MO) (b) show reduction in cerebellum and forebrain volume relative to control, uninjected zebrafish (a). Insets, images of the cerebellum highlighting loss of molecular and internal granular layers in the morphant (arrowheads). (c–f) Compared to control, uninjected zebrafish (c), embryos with MO-based knockdown of *chmp1a* (d) show reduced head size, with the hindbrain more markedly reduced in thickness (asterisks). This effect is similar to that seen with knockdown of the zebrafish orthologs of *BMI1*, *bmi1a* and *bmi1b* (e). When the *cdkn2a* MO is co-injected with the *chmp1a* MO, the *chmp1a* knockdown phenotype is partially rescued (f). (g) Control or morphant embryos were classified 28 hours post-fertilization (h.p.f.) as normal, disrupted or severely disrupted (Online Methods). The number above each bar is the total number of embryos examined. * $P < 0.001$, two-tailed Pearson's χ -squared test. (h,i) In sagittal cross-sectional areas from the mouse cerebellum at P25, *Bmi1*^{+/-} mice (i) have markedly reduced cerebellum size relative to *Bmi1*^{+/-} mice (h), although foliation and the structure of the lobules (indicated by roman numerals) are generally preserved. Representative scale bars, 200 μ m in a,c; 500 μ m in h.



body protein^{1,3}. CHMP1A was originally identified as a binding partner of the Polycomb group protein Pcl (Polycomblike)³. In the nucleus, it has been suggested to recruit the Polycomb group transcriptional repressor BMI1 to heterochromatin, and overexpressed CHMP1A has been shown to arrest cells in S phase³. In the cytoplasm, CHMP1A is part of the ESCRT-III complex^{1,2}. The ESCRT-III complex localizes to endosomes and interacts with VPS4A and VPS4B⁵ to assist in the trafficking of ubiquitinated cargo proteins to the lysosome for degradation⁶.

We investigated the potential effects of CHMP1A on Polycomb function by analysis of cell lines from two affected individuals harboring different *CHMP1A* mutations (CH3101 from family 1 and CH2401 from family 2), which show severely impaired doubling times compared to control cell lines, suggesting essential roles for CHMP1A in regulating cell proliferation (Fig. 2d). To examine BMI1 function in these cells, we performed quantitative PCR (qPCR) analysis of expression of the BMI1 target locus *CDKN2A*, which encodes alternative transcripts *INK4A* (also known as p16^{INK4A}; NM_000077) and *ARF* (also known as p14^{ARF}; NM_058195) in humans. This analysis revealed abnormally high expression of *INK4A*, the isoform implicated in cerebellar development, but not of *ARF* (Fig. 2e), suggesting derepression of *INK4A*. Chromatin immunoprecipitation (ChIP) with an antibody to BMI1 in control cell lines showed an approximately eightfold enrichment of BMI1 binding at *INK4A* promoter DNA relative to a control region 7 kb upstream, whereas cells from an affected individual (CH2401) showed only approximately half this enrichment in BMI1 binding (Fig. 2f). Enrichment of BMI1 at the *ARF* promoter was not substantial in this assay and was similar in both control cells and cell lines from affected individuals, consistent with the specificity of regulation of the *INK4A* isoform by BMI1 (Fig. 2f). Bmi1 has been shown to suppress the *Cdkn2a* locus and be required for neural stem cell self-renewal⁷. Our evidence suggests a role for CHMP1A in mediating BMI1-directed epigenetic silencing at the *INK4A* promoter but not at the *ARF* promoter.

We further explored the relationship between CHMP1A and BMI1 using morpholino-based knockdown experiments in zebrafish. Knockdown of the zebrafish *CHMP1A* ortholog (*chmp1a*; NM_200563) resulted in reduced cerebellum and forebrain volume compared to control, uninjected zebrafish, similar to the effects of human *CHMP1A* mutations and knockdown in zebrafish of *BMI1* orthologs (*bmi1a*, NM_194366, and *bmi1b*, NM_001080751; Fig. 3a–e and Supplementary Figs. 3 and 4). A second morpholino targeting *chmp1a* led to a similar phenotype, and both morpholinos were partially rescued by the introduction of human *CHMP1A* mRNA, confirming morpholino specificity (Supplementary Fig. 4). The cerebellum consists of five major cell types, with the principal cell, known as the Purkinje cell, deriving from the ventricular epithelium, whereas granule cells derive from a separate progenitor pool known as the rhombic lip. Granule cell precursors then migrate over the outer surface of the cerebellum and form the external germinal layer (EGL) before migrating radially past the Purkinje cells to settle in the internal granule layer (IGL)⁸. Within the *chmp1a*-morphant cerebellum, the internal granule and molecular layers were severely affected (Fig. 3a,b), which is consistent with the relatively preserved folia pattern of the human cerebellum (thought to primarily be established by Purkinje cells) and severely reduced volume (which is determined mainly by granule cell quantity).

We then tested genetic interactions between *chmp1a* and the zebrafish ortholog of *INK4A* (*cdkn2a*; XM_002660468). Knockdown of *cdkn2a* alone did not result in noticeable abnormalities, and double knockdown of *chmp1a* and *cdkn2a* resulted in partial rescue of the brain morphology defects seen with *chmp1a* knockdown (Fig. 3f,g). This rescue was analogous to the rescue of the *Bmi1*-knockout mouse cerebellar phenotype in *Bmi1*- and *Cdkn2a*-double knockout mice⁹. Of note, there were also parallels in brain morphology between individuals with *CHMP1A* mutations and *Bmi1*-deficient mice, which show cerebellar hypoplasia^{10,11} (Fig. 3h,i). In *Bmi1*-null mice, the cerebellar architecture was generally preserved, but the thickness of the granular and molecular layers was markedly reduced¹⁰, and *Bmi1*-deficient

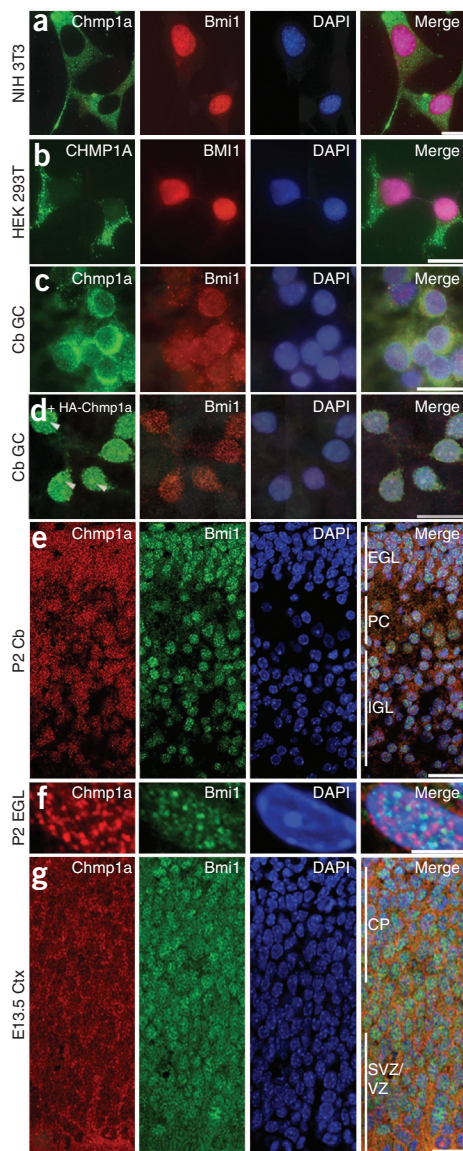


Figure 4 CHMP1A and BMI1 expression in cultured cells and the developing mouse brain. (a,b) Immunocytochemical analysis of NIH 3T3 cells (a) and HEK 293T cells (b). (c,d) Immunocytochemical analysis of mouse dissociated cerebellar granule cells (Cb GC) (c) and of these cells transfected with an expression construct encoding HA-tagged Chmp1a (d). Arrowheads indicate nuclear punctate staining for HA-Chmp1a. (e,f) Immunocytochemical analysis in mice of the developing cerebellum at P2 (P2 Cb) (e), P2 EGL cells (f) and the developing cerebral cortex at E13.5 (E13.5 Ctx) (g). EGL, external germinal layer; PC, Purkinje cells; IGL, internal granule layer; SVZ, subventricular zone; VZ, ventricular zone; CP, cortical plate. Scale bars, 20 μm in a–e,g; 5 μm in f.

mice show a modest reduction in cerebral volume^{10,12}, similar to individuals with *CHMP1A* mutations (Supplementary Note).

Subcellular localization of CHMP1A seems to vary depending on the cell type. Confocal images of NIH 3T3 cells showed prominent exclusion of Chmp1a from the nucleus (mouse *Chmp1a*, NM_145606), where Bmi1 was detected (Fig. 4a). In contrast, confocal images of HEK 293T cells, although also showing predominantly cytoplasmic localization of CHMP1A, showed some nuclear immunoreactivity as well (Fig. 4b). Primary cultures of cerebellar granule cells from mice also showed predominantly cytoplasmic localization of Chmp1a,

along with a speckled nuclear pattern (Fig. 4c). Overexpression of HA-tagged mouse Chmp1a in cultured granule cells resulted in abundant nuclear Chmp1a with a punctate expression pattern, confirming the speckled nuclear localization of endogenous Chmp1a (Fig. 4d) and consistent with earlier reports that CHMP1A can be present in the nucleus³. Even with Chmp1a overexpression, Chmp1a and Bmi1 do not prominently colocalize within the nucleus, which is also in agreement with previous data³.

Immunohistochemical studies of the developing cerebellum and cerebral cortex in mice revealed widespread expression of Chmp1a in dividing and postmitotic cells. Chmp1a immunoreactivity was seen in the nucleus and cytoplasm of EGL, Purkinje and IGL cells at postnatal day (P) 2 (Fig. 4e,f and Supplementary Fig. 5). In the nucleus of these cells, Chmp1a immunoreactivity was seen in a speckled pattern. These speckles may be seen adjacent to Bmi1 signals, but they usually did not colocalize (Fig. 4f and Supplementary Fig. 5). At later stages of cerebellar development (P4, P10 and P29), Chmp1a expression persisted in Purkinje and granule cells (Supplementary Fig. 6). Embryonic day (E) 13.5 cerebral cortex showed widespread Chmp1a expression in the neuroepithelial cells (Fig. 4g). In the postnatal cerebral cortex (at P4, P10 and P29), Chmp1a expression in postmitotic neurons of the cortical plate gradually decreased and became almost undetectable by P29 (Supplementary Fig. 6). These expression studies confirm that Bmi1 and Chmp1a are often expressed in the same cells. However, the absence of widespread subcellular colocalization of Bmi1 and Chmp1a suggests that the regulation of Bmi1 by Chmp1a is perhaps not mediated by direct physical interaction.

Our data implicate CHMP1A as an essential central nervous system regulator of BMI1, which in turn is a key regulator of stem cell self-renewal. The dual cytoplasmic and nuclear localization of CHMP1A and its connection to the ESCRT-III complex position CHMP1A as a potentially crucial link between cytoplasmic signals and the global regulation of stem cells via the Polycomb complex.

URLs. UCSC Human Genome Browser, <http://genome.ucsc.edu/>; Primer3, <http://frodo.wi.mit.edu/primer3/>; NetGene2, <http://www.cbs.dtu.dk/services/NetGene2/>; dbSNP, <http://www.ncbi.nlm.nih.gov/projects/SNP/>; 1000 Genomes Project, <http://www.1000genomes.org/>; NHLBI Exome Sequencing Project, <http://evs.gs.washington.edu/EVS/>.

METHODS

Methods and any associated references are available in the online version of the paper.

Note: Supplementary information is available in the online version of the paper.

ACKNOWLEDGMENTS

We thank the individuals and their families reported herein for their participation in this research. We thank M. van Lohuizen (Netherlands Cancer Institute) for providing the *Bmi1*-knockout mice, A. Wagers for help with breeding the *Bmi1*-knockout mice and P. Baas for sharing human DNA samples. This research was supported by grants from the US National Institute of Neurological Disorders and Stroke (NINDS; R01NS035129) and the Fogarty International Center (R21TW008223) to C.A.W., the Dubai Harvard Foundation for Medical Research, the Simons Foundation and the Manton Center for Orphan Disease Research. G.H.M. was supported by the Young Investigator Award of the National Alliance for Research on Schizophrenia and Depression (NARSAD) as a NARSAD Lieber Investigator. V.S.G. is supported by the Medical Scientist Training Program of Harvard Medical School, with financial support from the US National Institute of General Medical Sciences (NIGMS). C.A.W. and L.I.Z. are investigators of the Howard Hughes Medical Institute. Microscopy and image analyses were performed with support from the Cellular Imaging Core of the Boston Children's Hospital Intellectual and Developmental Disabilities Research Center.

AUTHOR CONTRIBUTIONS

G.H.M. designed the study, interpreted clinical information and brain MRIs, identified the disease locus, helped sequence candidate genes, analyzed the sequencing data to identify *CHMP1A* mutations, helped analyze the functional data and wrote the manuscript. V.S.G. performed RT-PCR, protein blots, mouse histology and immunohistochemistry, qPCR, ChIP and zebrafish morpholino experiments and wrote the manuscript. M.I.d.M. and H.D. ascertained family 1 and provided clinical information. K.D.A. performed zebrafish protein blots and mouse immunohistochemistry. K.L.K. performed the morpholino injections. H.-T.H. and L.I.Z. assisted with the morpholino experiments. R.S.H. helped organize genetic data and calculate LOD scores. J.M.F. and D.G. organized human samples and helped perform sequencing experiments. D.R. organized human samples and helped perform microsatellite analysis. A.D.H. assisted in immunohistochemical studies and imaging. A.N.M. assisted in ChIP. B.J.B. and J.N.P. organized clinical information and human samples. W.-H.T. and L.J.G. provided clinical information for family 3. A.J.B. interpreted the brain MRIs of the affected individuals. W.B.D. ascertained family 2 and provided clinical information. C.A.W. directed the overall research and wrote the manuscript.

COMPETING FINANCIAL INTERESTS

The authors declare competing financial interests: details are available in the [online version of the paper](#).

Published online at <http://www.nature.com/doi/10.1038/ng.2425>.

Reprints and permissions information is available online at <http://www.nature.com/reprints/index.html>.

- Howard, T.L., Stauffer, D.R., Degin, C.R. & Hollenberg, S.M. CHMP1 functions as a member of a newly defined family of vesicle trafficking proteins. *J. Cell Sci.* **114**, 2395–2404 (2001).
- Tsang, H.T. *et al.* A systematic analysis of human CHMP protein interactions: additional MIT domain-containing proteins bind to multiple components of the human ESCRT III complex. *Genomics* **88**, 333–346 (2006).
- Stauffer, D.R., Howard, T.L., Nyun, T. & Hollenberg, S.M. CHMP1 is a novel nuclear matrix protein affecting chromatin structure and cell-cycle progression. *J. Cell Sci.* **114**, 2383–2393 (2001).
- 1000 Genomes Project Consortium. A map of human genome variation from population-scale sequencing. *Nature* **467**, 1061–1073 (2010).
- Stuchell-Brereton, M.D. *et al.* ESCRT-III recognition by VPS4 ATPases. *Nature* **449**, 740–744 (2007).
- Scita, G. & Di Fiore, P.P. The endocytic matrix. *Nature* **463**, 464–473 (2010).
- Molofsky, A.V. *et al.* Bmi-1 dependence distinguishes neural stem cell self-renewal from progenitor proliferation. *Nature* **425**, 962–967 (2003).
- Garel, C., Fallet-Bianco, C. & Guibaud, L. The fetal cerebellum: development and common malformations. *J. Child Neurol.* **26**, 1483–1492 (2011).
- Jacobs, J.J., Kieboom, K., Marino, S., DePinho, R.A. & van Lohuizen, M. The oncogene and Polycomb-group gene *bmi-1* regulates cell proliferation and senescence through the *ink4a* locus. *Nature* **397**, 164–168 (1999).
- Leung, C. *et al.* Bmi1 is essential for cerebellar development and is overexpressed in human medulloblastomas. *Nature* **428**, 337–341 (2004).
- van der Lugt, N.M. *et al.* Posterior transformation, neurological abnormalities, and severe hematopoietic defects in mice with a targeted deletion of the *bmi-1* proto-oncogene. *Genes Dev.* **8**, 757–769 (1994).
- Zencak, D. *et al.* *Bmi1* loss produces an increase in astroglial cells and a decrease in neural stem cell population and proliferation. *J. Neurosci.* **25**, 5774–5783 (2005).

ONLINE METHODS

Genetic screening. The genetic study was approved by the Institutional Review Boards of Boston Children's Hospital and the University of Chicago. Appropriate informed consent was obtained from all involved human subjects.

The affected individuals and their parents from family 1 and the affected individuals from family 2 were subjected to genome-wide SNP screening with the Affymetrix GeneChip Human Mapping 250K Sty Array, performed at the Microarray Core of the Dana-Farber Cancer Institute. Microsatellite markers for fine mapping were identified using the UCSC Human Genome Browser¹³ and were synthesized with fluorescent labels (Sigma-Genosys). Two-point and multipoint LOD scores were calculated using Allegro¹⁴, assuming recessive inheritance with full penetrance and a disease allele frequency of 0.001. Sequencing primers were designed using Primer3 (ref. 15), and genomic DNA was sequenced using standard Sanger technology. Control DNA samples from neurologically normal individuals of European descent were obtained from the Coriell Cell Repositories (Coriell Institute for Medical Research). All nucleotide numbers are in reference to *CHMP1A* isoform 2 cDNA (NM_002768, with A of the ATG start site corresponding to +1) from the UCSC Genome Browser.

Analysis of *CHMP1A* splicing. Splice prediction software NetGene2 (ref. 16) was used to determine the effect of the family 1 allele on *CHMP1A* splicing. Epstein-Barr virus (EBV)-transformed lymphocytes were grown in RPMI-1640 (Gibco) with 15% FBS (Gibco) and 1% penicillin/streptomycin in (Lonza) a humidified incubator at 37 °C in 5% CO₂. RNA was isolated using the RNeasy Mini kit (Qiagen). Total RNA (5 µg) was used for first-strand synthesis with oligo(dT) primers and SuperScript III First-Strand Synthesis SuperMix (Invitrogen), and 1 µl of the product was used for the subsequent PCR reaction, with primers mapping from the 5' UTR to exon 6 of *CHMP1A* (NM_002768). Primer sequences are listed in **Supplementary Table 1**.

Proliferation assay of lymphoblastoid cell lines. EBV-transformed lymphoblastoid cell lines from eight control subjects and two affected individuals (CH2401 and CH3101) were grown. For each cell line, 2 × 10⁷ cells were grown, and 1 × 10⁶ cells were aliquoted into 4 sets of 5 T25 flasks filled with 10 ml of medium. Each set was allowed to grow for 24, 48, 72 and 96 h. Cell densities were estimated using a hemocytometer.

qPCR. EBV-transformed lymphoblastoid cell lines were grown, and cDNA was generated. *INK4A* and *ARF* levels were quantified using the StepOnePlus Real-Time PCR System (Applied Biosystems) with *GAPDH* as a control. Primer sequences are listed in **Supplementary Table 1**.

ChIP assays. ChIP was assayed as previously described¹⁷ with some modifications. For a single experiment, 2 × 10⁷ EBV-transformed lymphoblastoid cells and 4 µg of the antibody to BMI1 (Abcam, ab14389) were used. qPCR reactions were performed using SYBR Green reagents (Applied Biosystems) and the StepOnePlus Real-Time PCR System. Primers were assessed for specificity by analysis of their melt curves, and a standard curve was determined using four tenfold serial dilutions for each primer using the input DNA samples. The standard curve from the input DNA was determined using 3 µl from each serial dilution as a template. Fold enrichment for each ChIP sample was determined by using 3 µl from each sample as a template and comparing the resultant amplification to the standard curve for that primer pair. Primer sequences are listed in **Supplementary Table 1**.

Zebrafish morpholino experiments. ATG-targeting morpholinos were designed against *chmp1a* (*chmp1a* MO 1), *bmi1a*, *bmi1b* and the *INK4A* zebrafish ortholog (*cdkn2a*) (Gene Tools). In all experiments where *bmi1* morpholinos were used, *bmi1a* and *bmi1b* were injected together. Injections were performed at the one-cell stage. Optimal doses for the *chmp1a* MO 1, *bmi1a* and *bmi1b*, and *cdkn2a* morpholinos were 4.5, 1.2 and 4.0 ng, respectively. At 28 h.p.f., the embryos were visualized using a stereo microscope (Zeiss). To confirm the specificity of the effects of the *chmp1a* MO 1 morpholino, a second ATG-targeting *chmp1a* morpholino (*chmp1a* MO 2) was designed. For this experiment, the dosages of injected *chmp1a* MO 1 and *chmp1a* MO 2 were 6.0 and 3.0 ng, respectively. Morpholino sequences are listed in **Supplementary Table 1**.

For the rescue experiment, morphants were screened at 28 h.p.f. and scored for the presence of a defect in the angle of the head to the tail (measured at the otic vesicle) or a deviation in the straightness of the tail¹⁸. Human *CHMP1A* cDNA was PCR amplified from control human lymphoblastoid cell total RNA. Primer sequences are listed in **Supplementary Table 1**. The PCR product was subcloned into the pCS2+ vector, and 5'-capped mRNA was synthesized *in vitro* using the mMESSAGE kit (Ambion). mRNA was diluted in 0.1 M KCl and was titrated for the rescue experiments.

For histological preparation, morphants were grown at 28 °C for 5 d, fixed overnight at 4 °C in paraformaldehyde (PFA) and embedded in 3% low-melt agarose blocks (in PBS), which were fixed again in 4% PFA in PBS overnight. The fixed agarose blocks were embedded in paraffin and sectioned at 5-µm thickness in the sagittal plane. Sections were stained by standard techniques with hematoxylin and eosin and were visualized using a bright field microscope (Nikon).

For protein blotting, zebrafish embryos were harvested at 48 h.p.f. They were dechorionated and delinked as described¹⁹ and treated with lysis buffer (10% SDS and 0.5 M EDTA in 1× PBS) containing Complete Mini Protease Inhibitor Cocktail (Roche). Lysates were mixed with 2× Laemmli sample buffer, loaded onto a NuPage 4–12% Bis-Tris gel (Invitrogen) and run at 100 V for 2 h. Proteins were wet transferred onto Immobilon-P transfer membrane (Millipore) at 300 mA for 1.5 h at 4 °C. The membrane was blocked with Odyssey Blocking Buffer (LI-COR) and was incubated first with antibodies against Chmp1a (1:100 dilution; Abcam, ab104103) and β-actin (1:10,000 dilution; Abcam, ab6276) and then with IRDye secondary antibodies (LI-COR, 926-32212 and 926-68023). The LI-COR Imaging System was used for imaging and quantification.

Immunocytochemistry and immunohistochemistry. NIH 3T3 and HEK 293T cells were grown in DMEM with 10% FBS and 1% penicillin/streptomycin and were fixed and stained with antibodies against Chmp1a (1:200 dilution; Abcam, ab36679) and Bmi1 (1:250 dilution; Abcam, ab14389) using standard techniques. Staining was visualized on a confocal microscope (Nikon).

All animal work was approved by Harvard Medical School, Beth Israel Deaconess Medical School and Boston Children's Hospital Institutional Animal Care and Use Committees.

Cerebellar granule neuron cultures from euthanized, P5 mouse pups were prepared as described²⁰. After dissociation, cell density was measured using a hemocytometer, and 1 × 10⁶ cells were plated on each poly-L-ornithine-coated coverslip with 500 µl of plating medium in a 24-well plate. After 1 d *in vitro* (d.i.v.) in a 37 °C incubator, 20 µl of 250 µM AraC (cytosine-1-β-D-arabino-furanoside) was added to each well to arrest mitosis of non-neurons. At 2 d.i.v., conditioned medium was collected from each well, and the wells were washed with DMEM. Cells were then transfected with the HA-Chmp1a mammalian expression construct (GeneCopoeia, EX-Mm15805-M06). Transfection solution (87.6 µl of HBSS and 4.4 µl of 2.5 M calcium chloride with 1.5 µg of plasmid DNA) was prepared at room temperature, and 35 µl of the transfection solution was added to a total of 400 µl of conditioned medium and then added to each well. After an additional 36 h (4 d.i.v.), cells were fixed with 4% PFA for 20 min at room temperature, washed with PBS and stained with antibodies against HA (1:100 dilution; Abcam, ab9110) and Bmi1 (1:250 dilution; Abcam, ab14389). Untransfected cells were processed similarly and were stained with antibodies against Chmp1a (1:200 dilution; Abcam, ab36679) and Bmi1.

Tissues were perfused with 4% PFA, dissected and fixed overnight in 4% PFA and were then embedded in paraffin and sectioned at 5- or 8-µm thickness. After rehydration of the slides in serial washes with xylene, 50% xylene in ethanol, 100% ethanol, 70% ethanol, 50% ethanol, 30% ethanol and finally in PBS, the slides were boiled in antigen-retrieval solution (Retrievagen A, BD Biosciences) for 8 min in the autoclave. Slides were blocked with PBS with 0.1% Triton X-100 supplemented with 1% donkey serum for 1 h at room temperature, and antibodies against Bmi1 (1:400 dilution; Millipore, clone F6), Chmp1a (1:300 dilution; Abcam, ab36679 and ab104103) or calbindin (Swant, CB300) were added in the blocking solution for overnight incubation at 4 °C. Slides were washed three times for 5 min per wash in PBS and were developed with secondary antibodies conjugated to Alexa-Fluor dyes (Invitrogen) for 1.5 h at room temperature. Slides were again washed three times for 5 min per wash in PBS and were mounted with Fluoromount-G

(Southern Biotech) containing DAPI (1:1,000 dilution) and visualized on a confocal microscope (Nikon) or fluorescence microscope (Zeiss). For E13.5 and P2 cerebral cortex, frozen section specimens were used. For frozen sections, heads of E13.5 mouse embryos were directly fixed in 4% PFA, and P2 pups were perfused with 2 ml of 1× PBS and then with 4 ml of 4% PFA in PBS, followed by overnight fixation in 4% PFA. They were then placed in gradually increasing sucrose solutions (10%, 15% and 30%), each overnight, for cryopreservation and were then embedded in optimum cutting temperature (OCT) compound (Sakura Finetek) and sectioned at 20- μ m thickness. The same antigen retrieval and staining procedure was used as for the paraffin-embedded sections.

13. Kent, W.J. *et al.* The human genome browser at UCSC. *Genome Res.* **12**, 996–1006 (2002).
14. Gudbjartsson, D.F., Jonasson, K., Frigge, M.L. & Kong, A. Allegro, a new computer program for multipoint linkage analysis. *Nat. Genet.* **25**, 12–13 (2000).
15. Rozen, S. & Skaletsky, H.J. Primer3 on the WWW for general users and for biologist programmers. in *Bioinformatics Methods and Protocols: Methods in Molecular Biology* (eds. Krawetz, S. & Misener, S.) 365–386 (Humana Press, Totowa, New Jersey, 2000).
16. Brunak, S., Engelbrecht, J. & Knudsen, S. Prediction of human mRNA donor and acceptor sites from the DNA sequence. *J. Mol. Biol.* **220**, 49–65 (1991).
17. Flavell, S.W. *et al.* Genome-wide analysis of MEF2 transcriptional program reveals synaptic target genes and neuronal activity-dependent polyadenylation site selection. *Neuron* **60**, 1022–1038 (2008).
18. Kimmel, C.B., Ballard, W.W., Kimmel, S.R., Ullmann, B. & Schilling, T.F. Stages of embryonic development of the zebrafish. *Dev. Dyn.* **203**, 253–310 (1995).
19. Link, V., Shevchenko, A. & Heisenberg, C.P. Proteomics of early zebrafish embryos. *BMC Dev. Biol.* **6**, 1 (2006).
20. Bilimoria, P.M. & Bonni, A. Cultures of cerebellar granule neurons. *CSH Protoc.* **2008**, pdb prot5107 (2008).